scientific reports

Check for updates

OPEN

# Fine description of natural fractures in the tight sandstone reservoir of the Yanchang reservoirs in the southern Ordos Basin

Hongjian Wu[1,2]✉ & Xiangwei Kong[1,2]✉

**The Ordos Basin in China hosts substantial tight sandstone gas resources, characterized by well-developed natural fractures resulting from multi-phase tectonic activities. These fractures significantly enhance porosity and serve as critical pathways for gas migration and storage. However, they also introduce complexities to hydraulic fracturing processes and influence numerical characteristics. To effectively explore and develop these reservoirs, it is imperative to conduct quantitative research on the fracture numerical characteristics of the Yanchang Formation tight sandstone reservoir. This study integrates field outcrop observations, core descriptions, thin section analyses, tectonic stress field studies, and other methods to characterize the quantitative features of the tight sandstone reservoir in the study area while elucidating fracture development characteristics and spatial distribution. Specifically, high-angle fractures predominantly exhibit dip angles exceeding 60° due to nearly vertical structures. Additionally, considering the varying influence of different lithologies on fracture development is essential. Quantifying the relationship between fracture spacing and rock thickness in the Yanchang Formation is crucial. At a microscopic level, shear-type and tensile-shear type fractures are relatively developed, with average micro-fracture densities of 0.62 and 1.59 $mm^{-1}$, respectively, and an average micro-length value of approximately 0.00065 m, with widths ranging from 2 to 20 μm. Understanding the formation and distribution characteristics of natural fractures is vital for optimizing the development of low-permeability oil and gas fields and enhancing production through hydraulic fracturing.**

**Keywords** Tight sandstone gas, Natural fracture, Fracture dip and orientation, Facieology, Tectonic stress

With the continuous growth of global demand for oil and gas resources and the decline of conventional oil and gas production, unconventional oil and gas resources such as tight oil and gas, shale oil and gas, and coal seam gas have demonstrated significant potential under existing economic and technological conditions[1,2]. Their role in the global energy structure is increasingly vital, making them a cornerstone of the world's oil industry. Among these resources, tight sandstone gas holds substantial importance and is considered "the most promising and realistic important resource of the twenty-first century" in very low permeability and low porosity sandstone reservoirs[3,4]. The lithology of the sandstone reservoir is dense, brittle, commonly developing fractures. Natural fractures play a crucial role in enhancing pore connectivity within low permeability reservoirs, effectively improving their permeability, thus becoming a key determinant of production capacity[5,6].

The exploration of reservoir fractures originated from the development of specific fractured oil fields in the Middle East during the mid-twentieth century and experienced significant advancements in the 1970s, leading to the emergence of diverse perspectives and methodologies[7]. Natural fractures are influenced by a multitude of factors such as tectonic characteristics, sedimentary environment features, and rock properties, resulting in spatial distribution patterns that are challenging to predict[8]. Research approaches for low-permeability reservoir fractures have evolved from observational, statistical, and analytical studies of core and outcropping fractures to employing mathematical methods for simulating tectonic stress fields; from qualitative to quantitative research; and from simple to complex analyses[9–11]. Ghanbarian et al. (2022) studied the structural architecture and fold fault relationships of important areas in the central and southern parts of the Zagros hinterland through

[1]School of Petroleum Engineering, Yangtze University, Wuhan 430100, China. [2]Hubei Key Laboratory of Oil and Gas Drilling and Production Engineering, Yangtze University, Wuhan 430100, China. ✉email: 500712@yangtzeu.edu.cn; kongxw_yangtze@163.com

stereoscopic vision of aerial photographs, interpretation of satellite images, consideration of major ground terrain changes, and field research[12]. Later, through on-site inspections and microscopic thin section studies, using several indicators of motion shear significance, evidence of the development of the left lateral top of the northwest deformation zone was proposed[13]. Amirihanza et al. (2018) revealed the geological characteristics of the dual mode of extensional faults in the study block through the analysis of fault kinematics data[14,15].

Fracture identification primarily encompasses geological analysis, logging interpretation, and seismic assessment. Meanwhile, fracture number prediction utilizes methods including curvature analysis, binary classification techniques, fractal dimension calculations, numerical simulation of tectonic stress fields, as well as seismic and logging data integration[16–18].

As the exploration and development of oil and gas reserves has advanced, a significant number of fractured reservoirs and reservoirs controlled by fractures have been identified. In the field of reservoir fracture analysis and evaluation, there has also been substantial progress in related technical research[19,20]. Notably, the predictive method for structural fracture parameters based on geostress field simulation technology has made significant advancements[21–23]. Owing to the intricate nature of fracture development, many mathematicians utilize semi-quantitative concepts such as break rate and fracture development index to characterize the extent of fracture development in reservoirs.

The most commonly utilized methods for analyzing geological fractures include core observation, microscopic thin section analysis, and surface outcrop investigation. Additionally, CT scanning is employed. Core fracture observation involves naked-eye observation and statistical analysis to determine parameters such as strike, density, and aperture of fractures[24,25]. Thin section fracture analysis primarily focuses on reservoir micro-fractures, identifying their type, scale of development, and filling material through microscopic examination of thin sections. Surface outcrop investigation similarly aims to macroscopically observe and analyze fractures in order to comprehend the scale, morphology, and distribution characteristics of natural fractures within the study area[26]. This method establishes relevant geological models and a database of fracture parameter information to explore the developmental patterns and distribution of fractures[18,27]. Meanwhile, CT scanning utilizes computer reconstruction of ray information monitored by detectors to display two-dimensional images depicting internal density distribution within the core. It effectively presents fracture properties, filling conditions, and extension[28–30].

At present, there has been no comprehensive study on the natural fracture development characteristics of the Yanchang formation in the southern Ordos Basin. While these blocks generally exhibit natural fractures, the distribution patterns of fracture orientation, dip angle, density, and aperture remain unclear. The non-uniformity of fracture development distribution in the reservoir directly impacts drilling success rate and single well production capacity. Therefore, there is an urgent need to systematically predict the spatial distribution of reservoir fractures in this area under investigation. This thesis is based on surface outcropping rock fracture descriptions as well as core and cast thin section methods to elucidate the genesis types of Chang 6 reservoir natural fractures and quantitatively describe their parameters. It assesses distribution patterns longitudinally and laterally while analyzing their impact on production well deployment and development. This will provide a geological basis for efficient and rational development within this study area as well as contribute to improving oil recovery rates, which holds significant importance.

## Macroscopic description of natural fractures

This section presents a comprehensive examination and measurement of the exposed surface fractures within the study area's Yanchang formation, yielding a total of 261 valid fracture data points. To ensure the reliability of these measurements, approximately 10 readings are typically taken at each measurement location. The primary analysis, measurement, and characterization of the developed fracture system in the study area focus on the geometric morphology, spacing, characteristics, as well as strike and dip of the fractures.

### Structural stress field analysis

The cumulative effect of vector forces from distant, regional, and local sources forms the stress tensor, which exhibits varying strength and direction in both time and space. The Ordos Basin has experienced multiple tectonic movements since the Mesozoic era, including the Indus movement, Yanshan movement, and Xishan movement, resulting in significant alterations to the regional tectonic stress field's magnitude and orientation. In structural geology, the primary stress direction is typically determined by conjugate faults. If a given location or outcrop features intersecting faults with an X-shaped conjugate pattern, the maximum principal stress direction $\sigma_1$, intermediate principal stress direction $\sigma_2$, and minimum principal stress direction $\sigma_3$ can be calculated according to the Anderson model. Studies indicate that $\sigma_1$ aligns with the acute angle bisector of the fault angle; $\sigma_2$ aligns with the intersection line of two fault sets; and $\sigma_3$ aligns with the obtuse angle bisector.

The fracture system in the Yanchang formation reservoir of the study area's basin was developed under the influence of various tectonic stress fields and their collaborative effects during the Neogene. The research revealed that this fracture system was impacted by both Indus and Yanshan movements, with the former being the primary driver. By conducting field observations, classifying fractures, identifying Indus-period conjugate fractures, and employing polar stereographic projection for dynamic analysis, this study generated a stress axis orientation Table 1. Figure 1 illustrates that, in most instances, the predominant direction of maximum compressive stress during this period was NE, with an average orientation of 220° for the maximum principal stress direction. This reflects a prevailing NE-SW compression tectonic stress field at that time. For fractures formed during this period (as detailed in Table 1), it was observed that the dip angle $\sigma_1$ of the maximum principal stress axis is generally less than 10° while dip angle $\sigma_3$ of minimum principal stress axis ranges between 1° and 10°. Moreover, intermediate principal stress axis $\sigma_2$ typically exhibits a near-vertical state with an angle greater than 80° and runs parallel to bedding compression.

| Measurement point No | $\sigma_1$ | | $\sigma_2$ | | $\sigma_3$ | |
|---|---|---|---|---|---|---|
| | Position / ° | Dip angle / ° | Position / ° | Dip angle / ° | Position / ° | Dip angle / ° |
| 336 | 204 | 13 | 34 | 76 | 294 | 2 |
| 306 | 27 | 5 | 260 | 83 | 117 | 6 |
| 306–1 | 235 | 5 | 8 | 81 | 144 | 7 |
| 320 | 235 | 8 | 81 | 81 | 325 | 4 |
| 320–1 | 233 | 8 | 82 | 81 | 323 | 5 |
| 324 | 49 | 2 | 225 | 88 | 319 | 1 |
| 327 | 202 | 6 | 0 | 84 | 112 | 2 |
| 328 | 212 | 15 | 17 | 74 | 120 | 4 |

**Table 1**. Stress axis orientation of Indosinian period fractures.

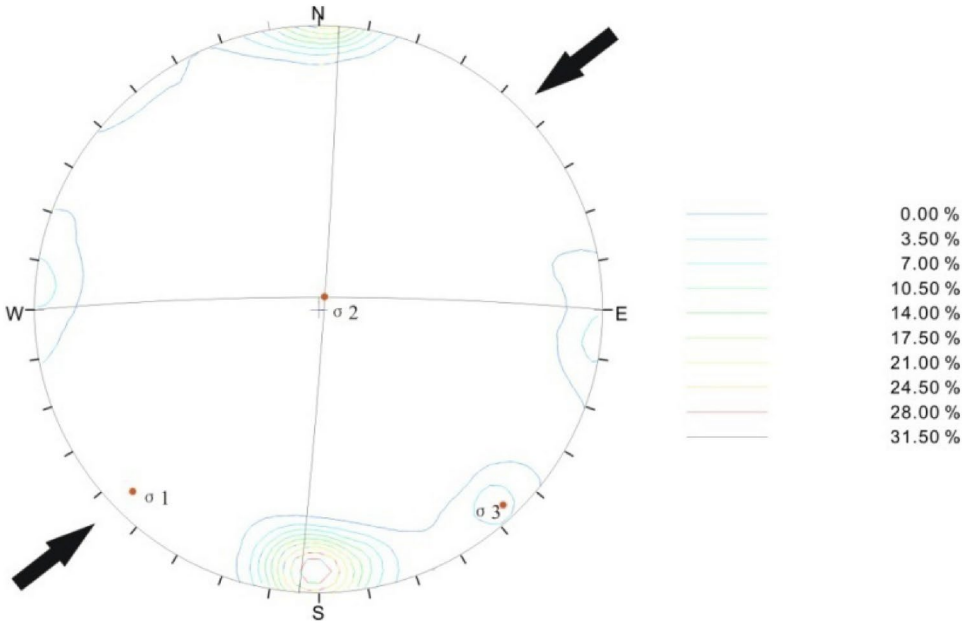


**Fig. 1**. Stress analysis diagram of the extended group in the study area.

In complex environments such as the Ordos Basin, where multiple tectonic phases are superimposed, the Anderson model has the following key limitations in determining the current stress direction. The multi-stage tectonic stress field interference in the Ordos Basin has undergone multiple tectonic transformations during the Indosinian period (NW–SE orientation), Yanshanian period (NE-SW), and Xishan period (near EW direction), resulting in: The proportion of ancient residual stresses reaching 15–38% of the current stress field (determined by acoustic emission Kessel effect). Currently, the direction of the stress field varies by 25–40° within a 20 km scale (microseismic monitoring data). Model assumption of uniform stress field and measured anisotropy index of geostress.

## Geometric characteristics of natural fractures

The study area is predominantly characterized by high-angle near-vertical structural fractures, with fracture dips generally exceeding 60°, and the majority of them surpassing 80°, approaching verticality (Fig. 2). Based on fracture dip, the study area fractures can be categorized into high-angle fractures constituting 95.61%, and low-angle fractures, accounting for 4.39%. Fractures with dip angles between 80° and 90° make up 65.93% of the total, those with dip angles between 70° and 80° account for 13.19%, while those between 60° and 70° represent 10.62%.

In the vertical direction, fractures typically undergo significant variations. Fractures exhibit well-developed features with a steep dip angle in sandstone, whereas they display a smaller dip angle or even disappear when extending into shale. Shale exerts a substantial constraining influence on fracture development in sandstone, leading to the initiation and termination of fractures within sandstone but not within shale. This phenomenon is closely linked to the mechanical parameters of the rock, with mineral content exerting a notable impact on brittleness coefficient. Rocks containing higher levels of quartz, feldspar, etc., tend to have an elevated brittleness coefficient and are more prone to natural fracture formation. Conversely, higher clay mineral content results in a

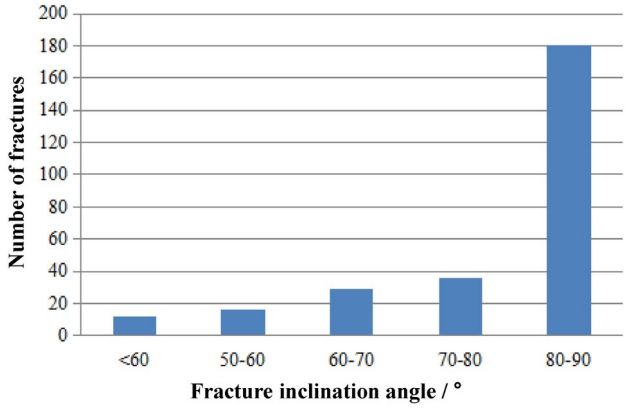


**Fig. 2**. Distribution characteristics of dip angles of structural fractures in the outcrop of the study area.

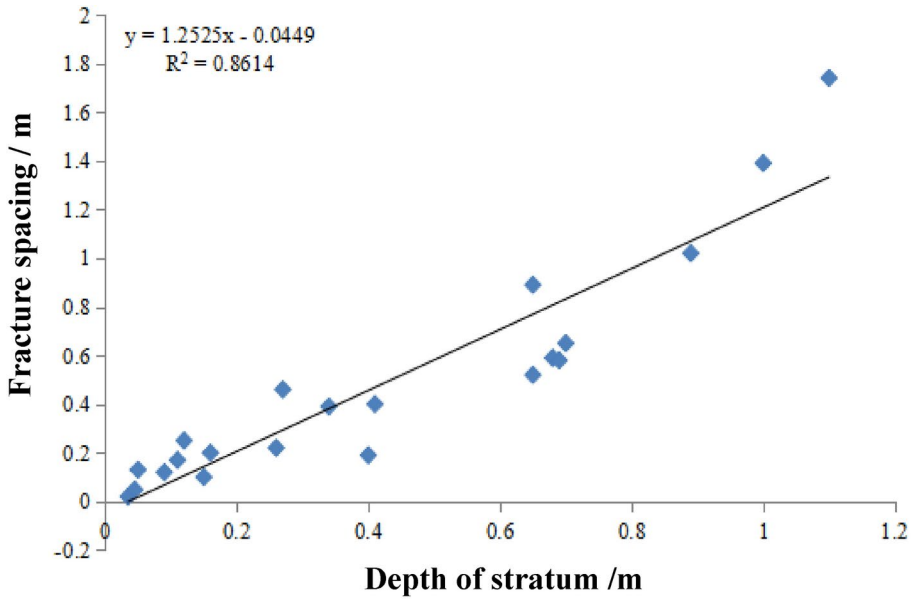


**Fig. 3**. Analysis of fracture spacing index.

lower brittleness coefficient and reduces the likelihood of natural fracture formation due to their strong plasticity during stress-induced deformation.

## Characteristics of natural fracture spacing

The slope of the linear function, with fracture spacing as the X-axis and mechanical layer thickness as the Y-axis, represents the fracture spacing index (FSI). The ratio of median fracture spacing to mechanical layer thickness is defined as the fracture spacing ratio (FSR). FSI indicates the intensity of fracture development in different layered rock formations, while FSR indicates the intensity of fracture development within a single mechanical layer. Larger values of FSI and FSR indicate more densely spaced fractures.

Following an investigation into how fracture spacing relates to layer thickness within formation layers, we introduced a fracture spacing index (FSI) as a representative measure. Figure 3 illustrates an FSI value of 1.252 while Table 2 presents calculated Fracture Spacing Ratio (FSR) values averaging at 1.06. The similarity between FSI and FSR values in Yanchang formation suggests that rock layer thickness predominantly controls fracture spacing.

In addition, the strong correlation coefficient (0.861) between rock layer thickness and fracture spacing indicates their close association across our study area. Linear relationships were evident among both individual and collective sets of fractures.

$$T = 1.252 * h - 0.044$$

where, $T$ is the average distance between fractures, m. $h$ is the thickness of a single rock layer, m.

| No | FSR | No | FSR |
|---|---|---|---|
| 1 | 1.25 | 8 | 1.75 |
| 2 | 2.10 | 9 | 0.58 |
| 3 | 1.15 | 10 | 0.80 |
| 4 | 0.63 | 11 | 0.87 |
| 5 | 0.64 | 12 | 1.18 |
| 6 | 1.18 | 13 | 0.87 |
| 7 | 0.71 | Average | 1.06 |

**Table 2**. Fracture spacing ratio (FSR) data.


**Fig. 4**. Shear fractures in the Triassic extended formation exposed on the surface.

## Natural fracture properties

Based on the cause of the fractures, the fractures in the study area can be categorized into structural and non-structural types. Structural fractures result from structural stress and represent permanent deformation caused by rock breakage under specific stress conditions. They typically arise from tectonic activity during reservoir formation and play a crucial role in reservoir development. Based on their mechanical properties, structural fractures can be further classified as tensile, shear, or tensile-shear types.

Shear fractures are formed under the influence of shear stress. The key characteristics of shear fractures in the study area include: (1) a stable dip, often exceeding 70° with minimal changes in both cross-sections and profiles, extending over a considerable distance, and exhibiting transverse fracture development. (2) The fracture surface is straight and smooth, displaying regular arrangement, with occasional evidence of shear sliding or steps. (3) Most fractures remain unfilled by other minerals and are in a closed state. (4) Shear fractures frequently exhibit the phenomenon of cutting through grains.

A compound fracture type known as the "Zhang shear joint" is formed due to the combined effects of tensile stress and shear stress, exhibiting characteristics of both tensile and shear fractures. This type of fracture typically features a larger aperture (Fig. 4a,b). Subsequent to the formation of natural fractures, they are often filled with various minerals during later stages of stress accumulation and geological fluid activity (Fig. 4c). Field observations indicate that the predominant filling minerals include calcite, quartz, and clay. The introduction of these minerals into the fractures alters the medium environment and frequently leads to dissolution.

There are also a few minor non-structural fractures with ambiguous formation patterns and uncertain directionality, contributing to an overall unstable trend. These curved fracture surfaces sometimes exhibit end branches or bifurcations. Furthermore, these fractures demonstrate limited extension and length due to rock properties. Upon analysis, it is inferred that the following types of non-structural fractures predominantly occur in the outcrops within the study area, weathering fractures resulting from rock weathering, contraction fractures formed during rock consolidation, particularly prevalent in rocks with high clay content.

## Analysis of the direction and period of structural fractures

Since the Mesozoic era, the Ordos Basin has experienced multiple tectonic movements, resulting in a complex stress field within the basin. The multi-stage tectonic stress has led to the development of numerous fracture systems in the Yanchang formation. These fracture systems are characterized by: (1) the presence of multiple sets of fractures with different strike orientations at the same location or within the same rock layer; (2) fractures with varying strike orientations within the same rock layer but at different locations. The orientation of all fractures in the Yanchang formation can be depicted using fracture strike rose diagrams (Fig. 5), fracture pole diagrams and fracture pole density diagrams (Fig. 6).

Analysis based on fracture distribution reveals four distinct fracture sets within Triassic strata at our research site: almost east–west orientation (85°- 95°), almost south-north orientation (0°–10°), NWW–SEE orientation

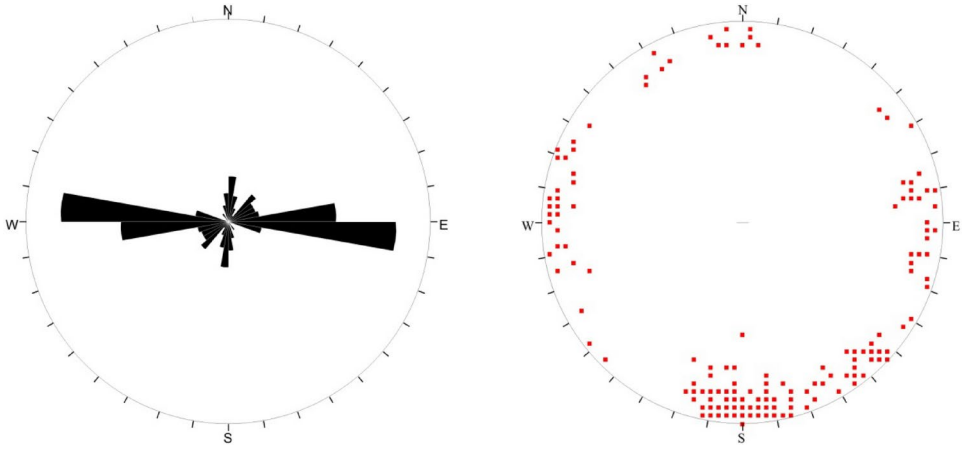


a. Number of fractures: 261 b. Maximum of 85 petals

**Fig. 5**. Rose diagram of fracture direction and fracture pole diagram of the extended group.

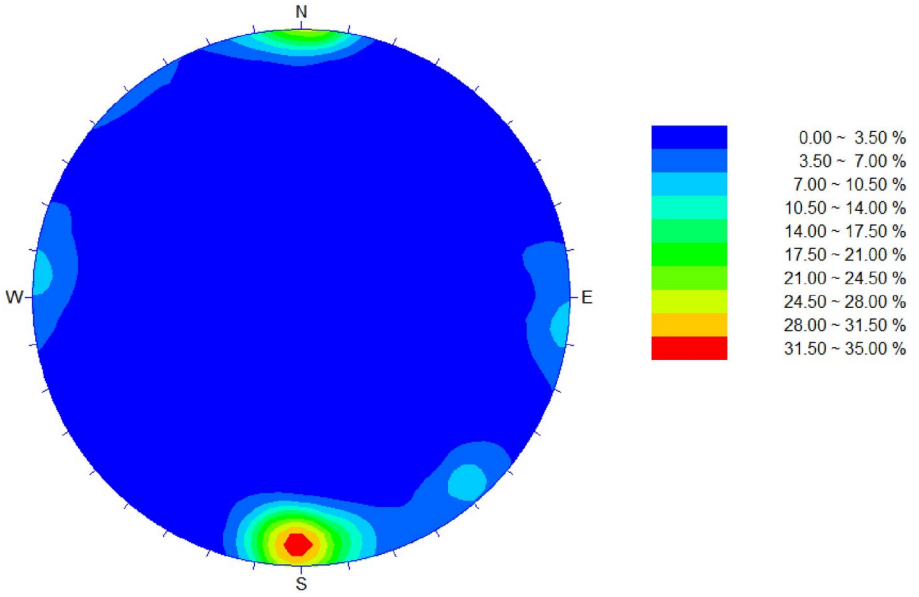


**Fig. 6**. Equivalent density map of fractures in the extended group (total number of fractures 261).

(300–310°), and NE-SW orientation (40°–50°) fracture systems. Notably, high-angle almost east–west-oriented fractures exhibit significant development with almost south-north-oriented ones following closely as depicted in Fig. 8. Conversely, those aligned with NW–SE and NNE—SSW orientations show comparatively lower development levels. This leads to a classification into two near-perpendicular systems—one aligning with almost east–west and almost south-north directions; while another aligns with NWW—SEE and NE—SW directions—based on regional tectonic stress field analysis alongside field observations.

Figures 7, 8, 9, 10 depict the rose diagram of fracture trends, the density diagram of fracture poles, and the iso-density diagram of fractures for both the Chang 6 and Chang 7 oil reservoir formations. It is evident that the primary fractures in these formations are predominantly oriented in an almost east–west direction, with a secondary set occurring in a nearly south-north direction. Stress analysis results were used to determine the stress state of the Indosinian Chang 6 and Chang 7 oil reservoir formations. The principal stress axes exhibit a northwest orientation (including both maximum and minimum principal stress axes). Given that our study area lies on the Yishan-Shaanxi slope of the Ordos Basin where strata are nearly horizontal, it can be observed that X-shaped or chessboard-style conjugate jointing axes on planes run parallel to intermediate principal stress axis. Consequently, within this entire plane stress field, northeast-directed compressive stress plays a pivotal role in shaping both near east–west and near south-north fracture systems. This also causes the intermediate principal stress axis of both formations to appear almost vertical, effectively creating what can be considered as a plane stress field.

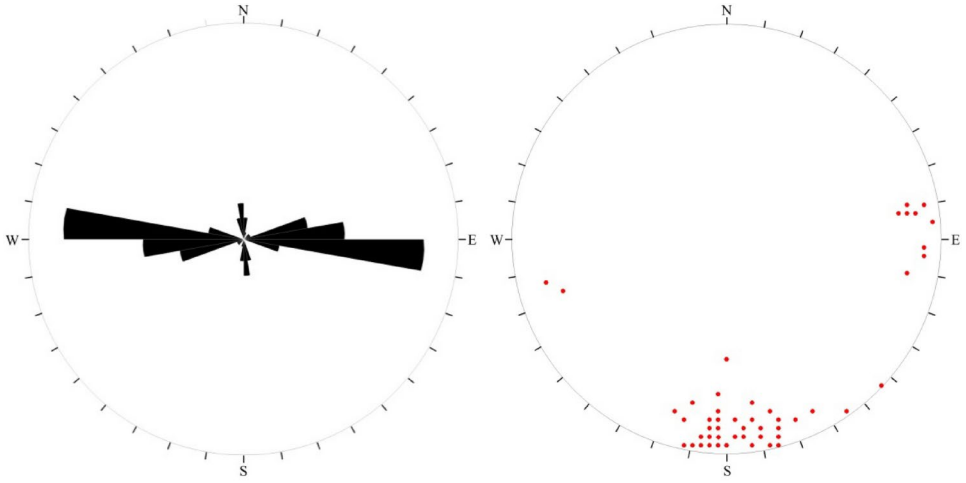


a. Number of fractures: 68 b. Maximum of 30 petals

**Fig. 7**. Rose diagram and fracture pole diagram of the fracture direction in the 6th oil reservoir group of the extension team.

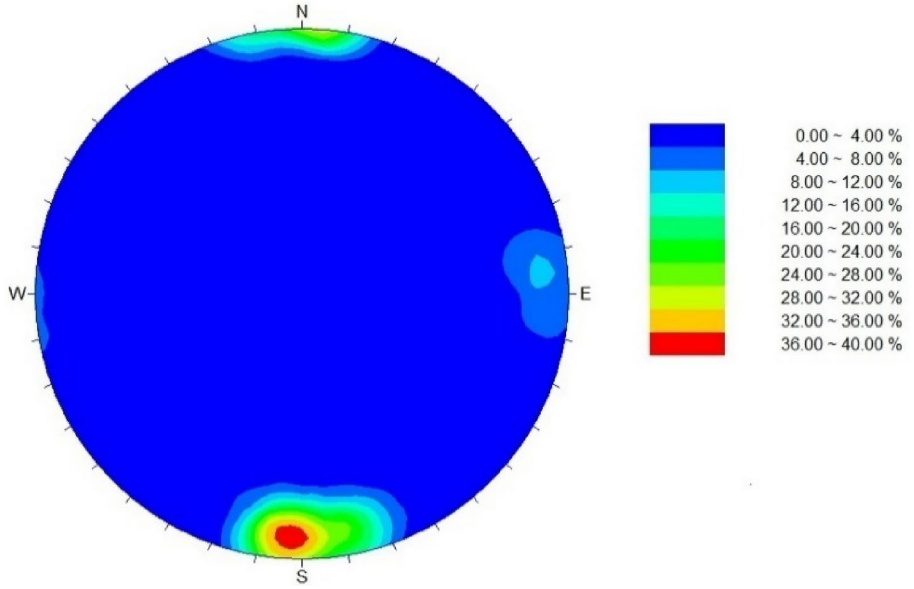


**Fig. 8**. Isodensity map of fractures in the 6th oil reservoir group of Yanchang Group (total number of fractures 68).

## Microscopic petrographic characteristics of natural fracture

### Analysis of diagenesis

Numerous thin section observations have demonstrated that the protracted diagenesis process in sedimentary rocks primarily encompasses compaction, cementation, dissolution, and fracturing types, which are interconnected and mutually influenced.

*Compaction and solution action*

Research suggests that the Yanchang formation in the study area experienced mechanical compaction during its early diagenesis stage when it was shallowly buried. The mineral particles in the reservoir primarily exhibit linear and face contacts (Fig. 11a,b). As a result of compaction, the original porosity of the reservoir is reduced, leading to deterioration in reservoir properties and impacting oil and gas permeability. Furthermore, dissolution directly contributes to the destruction of intergranular pores, resulting in a closer particle contact relationship under the combined influence of physical and chemical factors. With increasing stress on the particles over geological time, those subjected to dissolution will sequentially evolve from point contact to line contact,

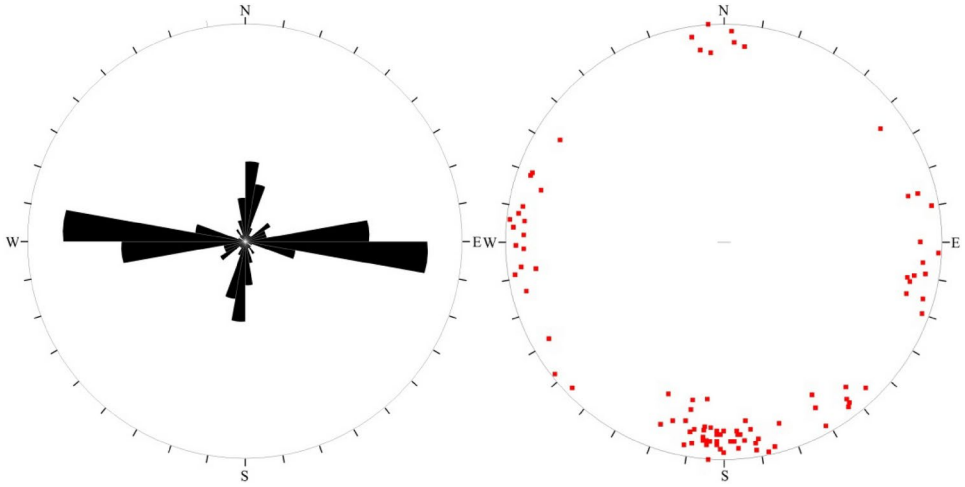


**Fig. 9**. Rose diagram and fracture pole diagram of the fracture direction in the 7th oil reservoir group of the extension team.

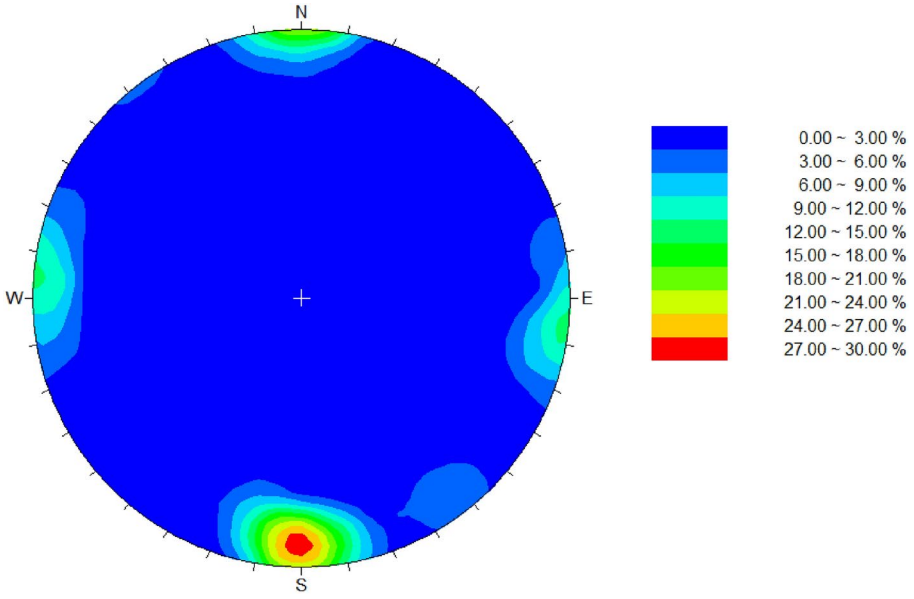


**Fig. 10**. Isodensity map of fractures in the 7th oil reservoir group of Yanchang Group (total number of fractures 68).

concave-convex contact, and finally suture line contact. In conclusion, compaction during diagenesis stands as one of the primary factors contributing to deteriorating reservoir properties.

*Cementation effect*

The cementing materials in the Yanchang Formation strata in the study area primarily consist of siliceous and calcareous cements. The cementing methods encompass secondary enlargement of mineral grains (Fig. 12b), clay linings around clastic particle edges, pore and intergranular cementation of mineral grains, among others. Microscopic observation reveals that the siliceous cementing material mainly comprises (1) various morphologies and orientations distributed between clastic particles (Fig. 12a); (2) secondary enlargement of quartz around clastic particles (Fig. 12b). Calcareous cementing material in the Yanchang formation predominantly manifests as intergranular bright crystal and polycrystalline cementation (Fig. 12c,d), accompanied by carbonate replacement of clastic particles. This calcareous cementing material obstructs sandstone pores, leading to a transition from originally high-quality sandstone to low-porosity and low-permeability sandstone over time (Fig. 12d).

*Metasomatism*

Research suggests that metasomatic processes in the regional extensional setting primarily involve: (1) carbonate mineral replacement of clastic grains, such as calcite replacing feldspar and clast grains, resulting in irregular

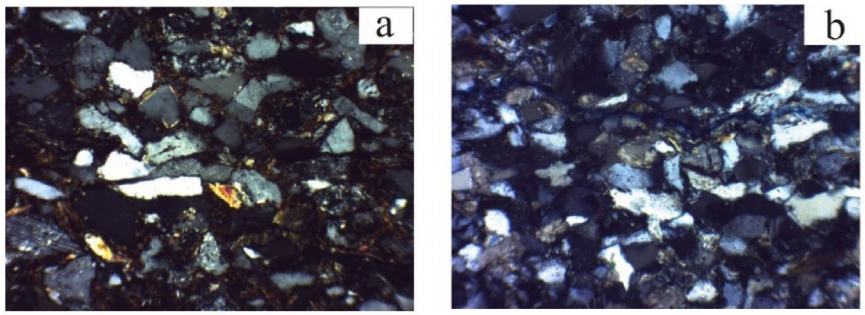


a. Line contact between quartz particles, 100 times,1575.00 m

b. Line contact and concave convex contact between quartz particles, 100 times, 1450.70 m

**Fig. 11**. Characteristics of compaction in the Chang 6 oil reservoir formation.

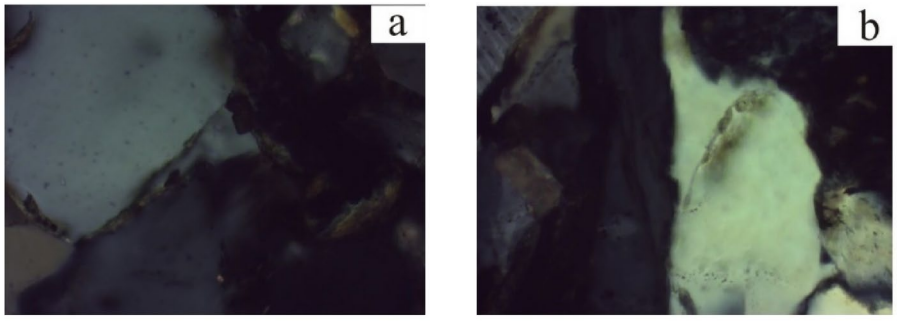


a. Siliceous cement between debris particles, 400 times

b. Quartz secondary enlarged edge, 400 times

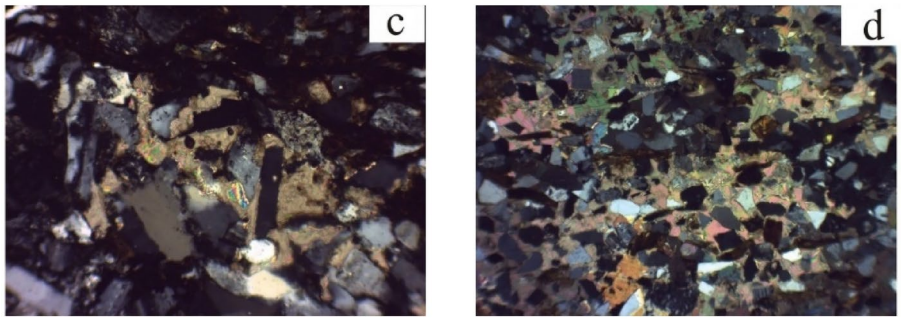


c. Bright crystal calcite cement, 100 times

d. Bright crystal calcite cement, 100 times

**Fig. 12**. Characteristics of cementation in Chang 7 oil reservoir group, 1450.70 m.

margins; and (2) clay mineral replacement of clastic grains, with illite and chlorite replacing mica, and illite also replacing plagioclase and other clastic grains with double-crystal bands or cleavage planes, or creating a bay-like margin on their edges (Fig. 13).

*Dissolution process*

Microscopic examinations have revealed extensive occurrences of dissolving processes within the Extended Group in our research area. Notably among these phenomena is a prominent dissolving pattern exhibited by various detrital particles (Fig. 14a), which precedes subsequent dissolutions involving feldspar and mica constituents. Alterations in fluid properties trigger destabilization within these detrital components resulting in their discernible morphological changes. Furthermore, we have predominantly observed dissolutions affecting feldspar as well as rock fragments within our study site; some particulates have entirely disintegrated forming

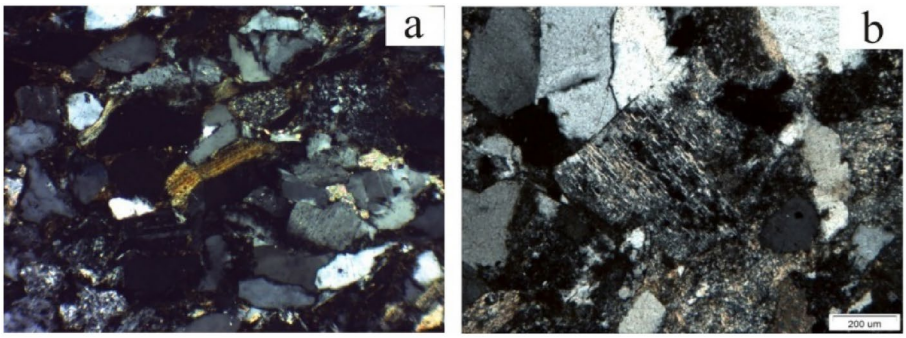


a. Illite replaced mica. 100 time

b. Illite replaced feldspar, 100 times

**Fig. 13**. Characteristics of metasomatism in the Chang 6 oil reservoir, 1628.64 m.

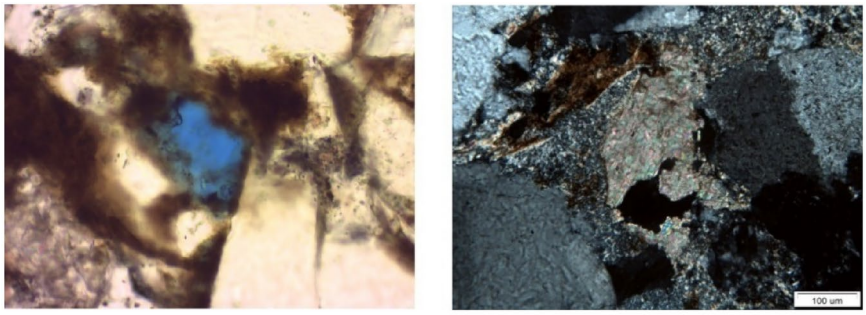


a. The debris particles are dissolved to form intergranular dissolution pores, with a magnification of 400 times

b. Calcium cement is dissolved to form dissolution pores, with a magnification of 100 times

**Fig. 14**. Characteristics of dissolution in Chang-7 oil reservoir formation, 1626.80 m.

cavity-like structures known as mold pores. Regarding cementation mechanisms, there has been substantial depletion primarily affecting calcium carbonate cements (Fig. 14b). Discharge-induced organic acid production has led to significant carbonates' dissolutions along with prolific pore formations. Our microscopic findings also demonstrate that most calcium-rich carbonate cements are susceptible to erosion while residual calcite and dolomite exhibit relative resilience preserving their cleavage patterns intact.

## Analysis of microfracture effects

The degree and extent of fracturing influence the rock permeability, which in turn governs reservoir connectivity and consequently impacts oil and gas productivity to a certain extent. Macro fractures encompass giant, large, medium, and small fractures observable in field outcrops and core samples; micro fractures typically exhibit smaller widths (< 0.01 mm) and lengths (< 0.01 mm) due to their diminutive size, often escaping naked eye detection but discernible under a microscope or scanning electron microscope.

*Development rate of micro fractures*

In the drilling cores and outcrops of the Yanchang Formation in the study area, particular attention was devoted to observing micro fractures. The rock lithology primarily comprises quartz sandstone, quartz-feldspar sandstone, clayey siltstone, siltstone with clay content, and mudstone. Statistical data indicate that 59% of the thin sections contain fractures while 41% do not; thus, the fracture occurrence rate is 59%. Micro fractures are generally well developed (Fig. 15), irrespective of whether they occur in sandstone or mudstone.

*Micro fracture properties*

Micro fracture types include structural fractures resulting from tectonic stresses that exhibit concentrated development with consistent trends, as well as diagenetic fractures associated with diagenesis processes. Based on their mechanical origins, we categorize the fractures within our study area as either tensile or shear fractures. Shear fractures form under shear stress without significant mineral infillings; they predominantly propagate vertically or at high angles with flat surfaces exhibiting distinct directional features. Typically, unfilled yet

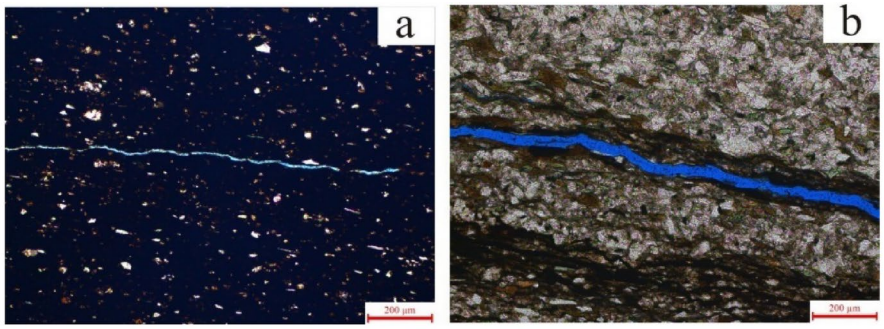


a. Micro fractures in mudstone, with a width of 2 μm and a length of Chang 6 oil layers

b. Micro fractures in feldspar lithic sandstone, with a width of 18 μm and a length of Chang 7 oil layers

**Fig. 15**. Comparison of fractures developed in mudstone and sandstone in the study area, 1081.23 m.

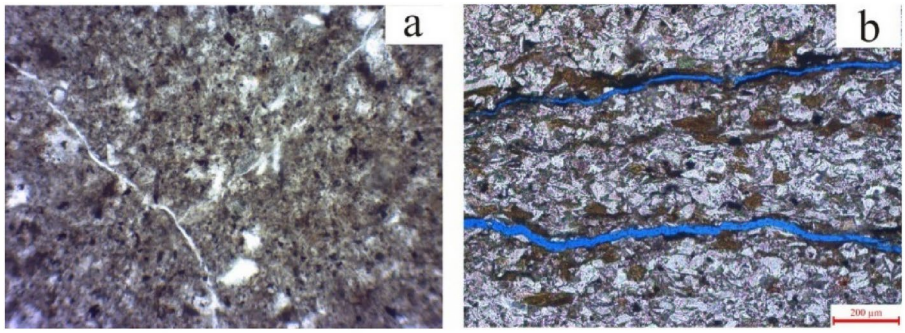


a. Micro fractures in mudstone, with a width of 2 μm

b. Micro fractures in feldspar lithic sandstone with wide fracture width 18 μm, 1253.56m

**Fig. 16**. Shear micro fractures in the Yanchang formation 1345.70 m.

effective, these fractures demonstrate stability along strike directions while aligning linearly or perpendicularly to one another (Fig. 16a). Some may contain calcite fillings arranged in parallel patterns within a single thin section (Fig. 16b).

*Development degree of micro fractures*

Under microscopic examination, it was observed that the micro fractures in the extended study area exhibited a width distribution primarily ranging from 0.6 to 20.0 μm, with some extending into the tens of microns. The surfaces of these fractures generally appear smooth and flat, often exhibiting parallel and perpendicular orientations. To more accurately investigate the developmental characteristics of these extended group fractures, the fracture lengths of 20 rock thin sections from the study area were statistically analyzed under a microscope, and their surface density was calculated.

The fracture surface density ($f_s$) is defined as the ratio of the total length of all fractures (L) on a given surface to the measured area (S). For thin plates with regular shapes, the area can be directly measured. However, for irregularly shaped thin plates, the surface area can be determined using transparent centimeter grid paper and statistical calculations of different types of fractures within that area. Subsequently, the following formula can be applied:

$$f_s = L / S$$

where, $f_s$—Fracture surface density, $m^{-1}$. $L$—Fracture length, m. $S$—Fracture area, $m^2$.

| Depth / m | Layer | Sample No | Fracture length / m | Total area of fractures / $m^2$ | Fracture surface density / $m/m^2$ |
|---|---|---|---|---|---|
| 1258.61 | Chang 7 | P 006 | 0.00114 | 0.000496 | 2.30 |
| 1254.47 | | P 007 | 0.00133 | 0.000436 | 3.05 |
| 1083.12 | Chang 6 | P 011 | 0.00025 | 0.000488 | 0.51 |
| 1080.75 | | P 013 | 0.00012 | 0.000503 | 0.24 |
| 1080.75 | | P 014 | 0.00033 | 0.000544 | 0.61 |
| 1498.09 | Chang 7 | X 007 | 0.00099 | 0.000506 | 1.96 |
| 1499.01 | | X 008 | 0.00081 | 0.000423 | 1.91 |
| 1405.00 | | X 009 | 0.00078 | 0.000403 | 1.94 |
| 1542.90 | | X 010 | 0.00072 | 0.000396 | 1.82 |
| 1376.83 | Chang 7 | X 011 | 0.00069 | 0.000406 | 1.70 |
| 1391.40 | Chang 6 | S 001 | 0.00025 | 0.000488 | 0.51 |
| 1396.47 | | S 002 | 0.00012 | 0.000503 | 0.24 |
| 1398.36 | | S 003 | 0.00023 | 0.000488 | 0.47 |
| 1444.50 | | S 004 | 0.00019 | 0.000503 | 0.38 |
| 1421.43 | | S 005 | 0.00021 | 0.000500 | 0.42 |

**Table 3**. Microscopic fracture statistics of the extended formation in the study area.

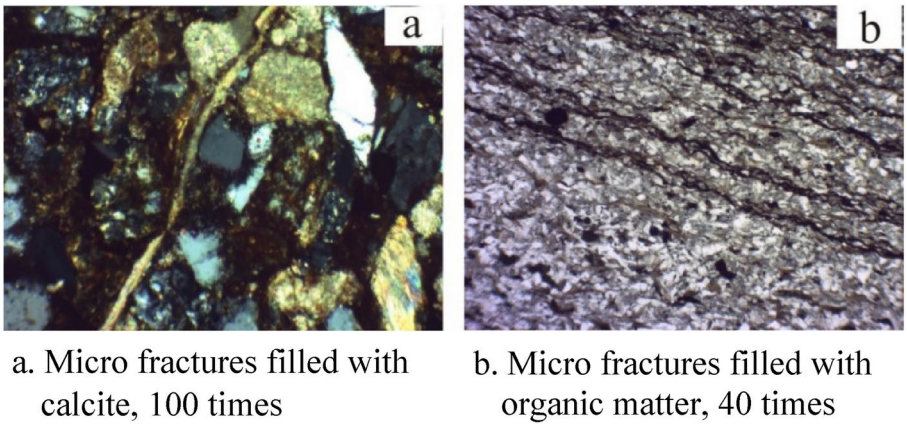


**Fig. 17**. Characteristics of unfilled micro fractures in the study area, 1347.03 m.

The fracture surface density of 28 microscopic rock samples in the study area was statistically determined, with values ranging from 0.17 to 3.05 $m/m^2$ and an average of 1.33 $m/m^2$ (Table 3). The Yanchang Formation exhibits a higher degree of fracture development, categorized as Level II. Furthermore, the fracture surface density of each oil layer group in the Chang 6 and Chang 7 observation wells was quantitatively analyzed under a microscope, revealing an average fracture surface density of 1.59 $m/m^2$ for the Chang 7 oil layer group and 0.62 $m/m^2$ for the Chang 6 oil layer group.

*Micro fracture filling type*

Micro fractures can be categorized into three groups based on their filling conditions: unoccupied (unfilled) micro fractures; completely occupied (fully filled) micro fractures; and partially occupied (semi-filled) micro fractures. Completely occupied micro fractures can be subcategorized into calcite-occupied (calcite-filled) micro fractures or organic material-occupied (organic-filled) micro fractures. Within the Yanchang formation studied here, unoccupied micro fractures constitute approximately 69% of all occurrences. These unoccupied microstructures are readily distinguishable under polarized light microscopy due to their lower contrast compared to quartz, feldspar, and other minerals; they exhibit similar optical characteristics to resin when viewed between crossed polarizers. Tensile unoccupied microstructures typically form a disordered network pattern with irregular surfaces and uneven edges. Shear unoccupied structures are more prevalent; they propagate linearly within rocks, sometimes intersecting grains. Thin sections display conspicuous molds, some containing penetrating voids. Shear unoccupied structures commonly occur within zones where there is an abrupt change in rock mechanical properties, resulting in distinctive shear fracturing at these intersections.

The fillings in fractures mainly consist of calcite and organic matter. Calcite fills the originally formed fractures (Fig. 17), and microscopic observations reveal that calcite and calcareous cementation occur almost simultaneously, originating from the same geological fluid period. Some thin sections exhibit organic

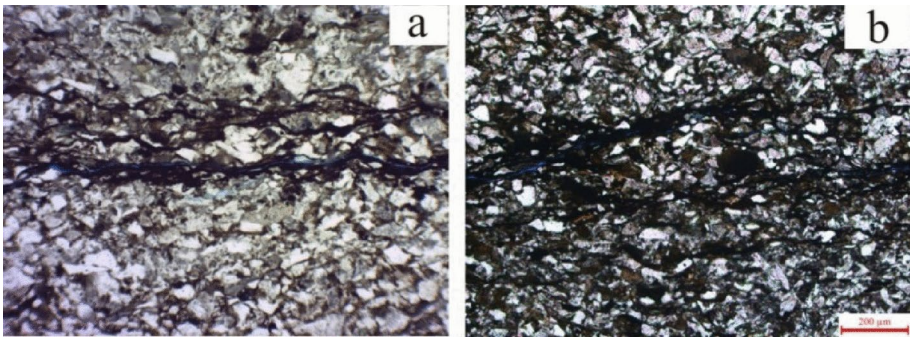


**Fig. 18**. Micro fractures that are not completely filled with organic matter, 40 times, 1547.41 m.

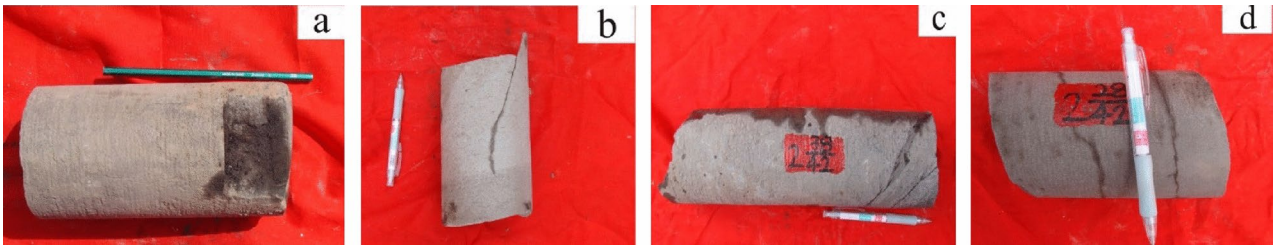


**Fig. 19**. Natural fracture characteristics in the underground rock core.

matter filling fractures, which appear in a parallel arrangement with semi-transparent or weakly translucent characteristics under a polarized light microscope. During the migration of organic matter through the fractures, light hydrocarbons are preferentially transported, while heavy hydrocarbons remain in unfilled fractures, ultimately leading to their complete filling.

The concept of a semi-packed fracture refers to a fracture morphology that falls between an unpacked fracture and a fully packed fracture, indicating that the original open fracture has not been completely filled with organic matter or other filler materials (Fig. 18). This observation serves as compelling evidence for the significant role played by fractures in oil and gas migration.

## Fracture characteristics on rock cores

The core observation results indicate that, within the formation's stress state, both structural and diagenesis-induced fractures display slightly open characteristics. Long fractures exhibit shear fracture features, typically with an inclination angle exceeding 80°. Upon release of ground pressure, all long fractures will break along the fracture surface, which is smooth and even. The core fractures can be primarily categorized into two types of geneses: structural fractures and diagenesis-induced fractures. Structural fractures are more prevalent, with a relatively flat dip and often occurring in a vertical or high-angle state. Diagenesis-induced fractures generally have smaller dip angles, usually less than 20°, and show slight openness after ground pressure release as they cut low-angle with the rock's bedding or cleavage. In some oil-bearing intervals, black residual oil is clearly observable, confirming the significant role of natural fractures in reservoir storage and migration (Fig. 19).

## Analysis of fracture causes

Since the Mesozo Ordos Basin has experienced multiple tectonic activities since the Cenozoic era, including the Indosinian movement, Yanshan movement, and the Xixian movement. Among them, the Indosinian tectonic movement is the main reason for the formation of the fractures in the southern part of the Yanchang exploration area. Previous studies have shown that during the Indosinian period, the southern part of the basin was mainly affected by a NE-SW compressive tectonic stress field, i.e., the maximum principal stress direction in the southern part of the Yanchang exploration area is NE-SW. According to the Anderson model, this stress field is the key factor in forming the near SN and near EW conjugate fracture systems. The entire study area is located on the Yishan-Shaanxi Slope, with a small dip angle and simple internal structures. Due to near horizontal distribution of maximum principal stress ($\sigma_1$) and minimum principal stress ($\sigma_3$) under remote action, this is a crucial reason for formation of large number high-angle fractures.

Throughout the Indo-Sinian tectonic movement period, the Ordos region was generally subjected to shear stress field, and the remote stress from the basin edge mainly presented a shear nature, which was the most direct cause of the formation of a large number of shear fractures in the Yanchang formation of the study area. After the Indo-Sinian tectonic movement, the direction and magnitude of the remote stress field produced by the Yanshan and Xizang tectonic movements changed, and some of the formed shear fractures were gradually transformed into a combination of tensile and shear fractures under the influence of newly generated tectonic

stress field. Tensile-shear fractures are composite fractures formed under combined action of tensile stress and shear stress, having both tensile and shear characteristics. In contrast, fewer tensile fractures developed in Yanchang formation study area. Only few tensile fractures were formed due to increase in internal pressure caused by fluid or formation new minerals during late diagenesis process.

The brittleness coefficient of rocks is significantly influenced by the mineral content. Elevated concentrations of minerals such as quartz and feldspar enhance the brittleness coefficient of rocks, facilitating the formation of natural fractures. Conversely, high levels of clay-like minerals diminish the brittleness coefficient of rocks, reducing the likelihood of natural fracture occurrence and contributing to the common presence of fractures in sandstone.

## Conclusion

(1) The southern part of the exploration area is predominantly influenced by the Indosinian and Yanshan movements, with the Indosinian movement being the primary factor in the formation of fractures in the Yanchang formation. Within the Chang 6 and Chang 7 oil-bearing formations, four sets of fractures have developed, encompassing nearly E-W orientations (85°–95°), nearly S–N orientations (0°–10°), NWW-SEE orientations (300°–310°), and NE-SW orientations (40°–50°). Among these, high-angle nearly E-W oriented fractures are most extensively developed, followed by nearly S–N oriented fractures.

(2) The extended group strata are all characterized by high-angle near-vertical structural fractures, with fracture dips generally exceeding 60°. Lithology exerts a significant influence on fracture development throughout the southern exploration area, as fractures tend to form in sandstone and cease in shale. Fracture spacing is primarily determined by rock thickness, with larger rock thicknesses corresponding to greater fracture spacing. A relationship of $T = 1.252\ h - 0.044$ exists between fracture spacing and rock thickness.

(3) The shear and tensile fractures in the Chang 6 and Chang 7 reservoir units exhibit well-developed characteristics, with the tensile fractures being relatively less developed. The stable shear fractures have a dip angle greater than 70°, appearing generally flat and smooth, predominantly unfilled by other minerals and in a closed state. These fractures form an X-shaped conjugate shear fracture system. Tensile-shear fractures display features of both tensile and shear fractures, typically having larger aperture sizes and often filled with calcite, quartz, and clay. Overall, the micro fractures can be categorized as unfilled, fully filled or semi-filled; the unfilled micro fractures play a positive role in enhancing the physical properties of the reservoir.

(4) The micro fractures within the Chang 6 and Chang 7 oil layers can be categorized into shear micro fractures and tensile micro fractures. Among these, shear micro fractures are predominant, with most remaining unfilled by other minerals. They primarily propagate vertically or at high angles over long distances, exhibiting straightness and specific structural and directional characteristics. These fractures demonstrate effective and stable orientation, generally aligning in parallel or perpendicular patterns. The overall micro fracture surface density across the entire Chang 6 and Chang 7 oil layers ranges from 0.17 to 3.05 $m/m^2$, averaging at 1.33 m $/m^2$. Based on fracture development evaluation standards, the fracture development within the Yanchang formation is relatively high, reaching level II. The average micro fracture surface density in the Chang 6 and Chang 7 oil layers is approximately 0.62 and 1.59 $m/m^2$ respectively; meanwhile, the average length of these fractures' measures about 0.00065 m with a width range of 2–20 μm.

## Data availability

The datasets used and/or analyzed during the current study available from the corresponding author on reasonable request.

Received: 3 August 2024; Accepted: 14 February 2025
Published online: 20 February 2025

## References

1. Jinxing, D., Yunyan, Ni. & Xiaoqi, Wu. Tight gas in China and its significance in exploration and exploitation. *Pet. Explor. Dev.* **39** (3), 277–284 (2012).
2. Jia, A. et al. Development status and prospect of tight sandstone gas in China. *Nat. Gas Ind. B* **9** (5), 467–476 (2022).
3. Khlaifat, A., Qutob, H., & Barakat, N. Tight gas sands development is critical to future world energy resources. In *SPE Middle East Unconventional Resources Conference and Exhibition* (SPE-142049). SPE. (2011).
4. Zou, C. et al. Tight gas sandstone reservoirs in China: characteristics and recognition criteria. *J. Petrol. Sci. Eng.* **88**, 82–91 (2012).
5. Ju, W. & Sun, W. F. Tectonic fractures in the Lower Cretaceous Xiagou Formation of Qingxi Oilfield, Jiuxi Basin, NW China. Part two: Numerical simulation of tectonic stress field and prediction of tectonic fractures. *J. Petrol. Sci. Eng.* **146**, 626–636 (2016).
6. Zeng, L. et al. Impacts of the tectonic stress field on natural gas migration and accumulation: a case study of the kuqa depression in the tarim basin, china. *Mar. Pet. Geol.* **27** (07), 1616–1627 (2010).
7. Edo, G. I. et al. Petroleum discovery, utilization and processing in the World and Nigeria: a comprehensive literature review. *Sustain. Chem. Eng.* https://doi.org/10.37256/sce.5120243970 (2024).
8. Cawood, A. J., Watkins, H., Bond, C. E., Warren, M. J. & Cooper, M. A. Natural fracture patterns at Swift Reservoir anticline, NW Montana: the influence of structural position and lithology from multiple observation scales. *Solid Earth* **14** (9), 1005–1030 (2023).
9. Shafiei, A., Dusseault, B. & M., Kosari, E., & N. Taleghani, M.,. Natural fractures characterization and in situ stresses inference in a carbonate reservoir—an integrated approach. *Energies* **11** (2), 312 (2018).
10. Liu, J. et al. Simulation of paleotectonic stress fields and quantitative prediction of multi-period fractures in shale reservoirs: a case study of the Niutitang Formation in the Lower Cambrian in the Cen'gong block, South China. *Mar. Petrol. Geol.* **84**, 289–310 (2017).
11. Viswanathan, H. S. et al. From fluid flow to coupled processes in fractured rock: Recent advances and new frontiers. *Rev. Geophys.* https://doi.org/10.1029/2021RG000744 (2022).
12. Ghanbarian, M. A., Yassaghi, A. & Derakhshani, R. Detecting a sinistral transpressional deformation belt in the Zagros. *Geosciences* **11** (6), 226 (2021).

13. Ghanbarian, M. A. & Derakhshani, R. The folds and faults kinematic association in Zagros. *Sci. Rep.* **12** (1), 8350 (2022).
14. Amirihanza, H., Shafieibafti, S., Derakhshani, R. & Khojastehfar, S. Controls on Cu mineralization in central part of the Kerman porphyry copper belt, SE Iran: constraints from structural and spatial pattern analysis. *J. Struct. Geol.* **116**, 159–177 (2018).
15. Rashidi, A. & Derakhshani, R. Strain and moment rates from GPS and seismological data in northern Iran: implications for an evaluation of stress trajectories and probabilistic fault rupture hazard. *Remote Sens.* **14** (9), 2219 (2022).
16. Lai, J. et al. A review on the applications of image logs in structural analysis and sedimentary characterization. *Mar. Petrol. Geol.* **95**, 139–166 (2018).
17. Maity, D. & Aminzadeh, F. Novel fracture zone identifier attribute using geophysical and well log data for unconventional reservoirs. *Interpretation* **3** (3), T155–T167 (2015).
18. Wilson, T. H., Smith, V. & Brown, A. Develo** a model discrete fracture network, drilling, and enhanced oil recovery strategy in an unconventional naturally fractured reservoir using integrated field, image log, and three-dimensional seismic data. *AAPG Bullet.* **99** (4), 735–762 (2015).
19. Bourbiaux, B. Fractured reservoir simulation: a challenging and rewarding issue. *Oil Gas Sci. Technol. Revue l'Institut Français Pétrol.* **65** (2), 227–238 (2010).
20. Gong, L. et al. Characterization, controlling factors and evolution of fracture effectiveness in shale oil reservoirs. *J. Petrol. Sci. Eng.* **203**, 108655 (2021).
21. Feng, J. et al. An improved geomechanical model for the prediction of fracture generation and distribution in brittle reservoirs. *PloS ONE* **13** (11), e0205958 (2018).
22. Hu, L. A review of mechanical mechanism and prediction of natural fracture in shale. *Arab. J. Geosci.* **15** (6), 474 (2022).
23. Liu, J. et al. Quantitative prediction of fractures using the finite element method: A case study of the lower Silurian Longmaxi Formation in northern Guizhou, South China. *J. Asian Earth Sci.* **154**, 397–418 (2018).
24. Cappuccio, F. *Image Analysis of X-Ray Computed Tomographic Datasets, Quantification of Porosity, and Applications to Understanding Fracturing of Rock Masses*. (Doctoral dissertation, University of Otago). (2021).
25. Sun, S. et al. Characterization of natural fractures in deep-marine shales: a case study of the Wufeng and Longmaxi shale in the Luzhou Block Sichuan Basin, China. *Front. Earth Sci.* **17** (1), 337–350 (2023).
26. Dashti, R., Rahimpour-Bonab, H. & Zeinali, M. Fracture and mechanical stratigraphy in naturally fractured carbonate reservoirs-A case study from Zagros region. *Mar. Petrol. Geol.* **97**, 466–479 (2018).
27. Laubach, S. E. et al. The role of chemistry in fracture pattern development and opportunities to advance interpretations of geological materials. *Rev. Geophys.* **57** (3), 1065–1111 (2019).
28. Kawakata, H. et al. Three-dimensional observations of faulting process in Westerly granite under uniaxial and triaxial conditions by X-ray CT scan. *Tectonophysics* **313** (3), 293–305 (1999).
29. Ueta, K., Tani, K. & Kato, T. Computerized X-ray tomography analysis of three-dimensional fault geometries in basement-induced wrench faulting. *Eng. Geol.* **56** (1–2), 197–210 (2000).
30. Zhang, H., Zhang, T., Pang, M., Wang, D. & Zeng, F. Space-time evolution characteristics of loaded gas-bearing coal fractures based on industrial μCT. *Rev. Adv. Mater. Sci.* **62** (1), 20230135 (2023).

## Author contributions
X. Kong: Conceptualization, funding acquisition, project administration, resources, writing—original draft and software. H. Wu: writing—original draft Project administration, resources, investigation, methodology, software, and visualization, conceptualization. All authors have read and agreed to the published version of the manuscript.

## Funding
This research was funded by "The Ministry of Science and Technology of Sinopec Project: Automatic linkage control technology for the drilling overflow of the fractured gas reservoir, grant number P22117) and Key Technology of Volume Fracturing for Medium shallow Tight Sandstone Gas Reservoirs in Western Sichuan, grant number P22017". The authors are grateful for the support of the National Natural Science Foundation of China.

## Declarations

## Competing interests
The authors declare no competing interests.

## Additional information
**Correspondence** and requests for materials should be addressed to H.W. or X.K.